Icarus 354 (2021) 114026

Contents lists available at ScienceDirect

Icarus

journal homepage: www.elsevier.com/locate/icarus

Assessing the survivability of biomarkers within terrestrial material impacting the lunar surface

Samuel H. Halim [a,*], Ian A. Crawford [a], Gareth S. Collins [b], Katherine H. Joy [c], Thomas M. Davison [b]

[a] Department of Earth and Planetary Sciences, Birkbeck, University of London, Malet St., London WC1E 7HX, UK
[b] Department of Earth Science & Engineering, Imperial College London, Kensington, London SW7 2AZ, UK
[c] Department of Earth and Environmental Sciences, University of Manchester, Oxford Rd., Manchester M13 9PL, UK

ARTICLE INFO

Keywords:
Moon, surface
Impact-processes
Cratering
Meteorites
Biomarkers

ABSTRACT

The history of organic and biological markers (biomarkers) on the Earth is effectively non-existent in the geological record >3.8 Ga ago. Here, we investigate the potential for terrestrial material (i.e., terrestrial meteorites) to be transferred to the Moon by a large impact on Earth and subsequently survive impact with the lunar surface, using the iSALE shock physics code. Three-dimensional impact simulations show that a typical basin-forming impact on Earth can eject solid fragments equivalent to $\sim 10^{-3}$ of an impactor mass at speeds sufficient to transfer from Earth to the Moon. Previous modelling of meteorite survivability has relied heavily upon the assumption that peak-shock pressures can be used as a proxy for gauging survival of projectiles and their possible biomarker constituents. Here, we show the importance of considering both pressure and temperature within the projectile, and the inclusion of both shock and shear heating, in assessing biomarker survival. Assuming that they survive launch from Earth, we show that some biomarker molecules within terrestrial meteorites are likely to survive impact with the Moon, especially at the lower end of the range of typical impact velocities for terrestrial meteorites (2.5 km s^{-1}). The survival of larger biomarkers (e.g., microfossils) is also assessed, and we find limited, but significant, survival for low impact velocity and high target porosity scenarios. Thermal degradation of biomarkers shortly after impact depends heavily upon where the projectile material lands, whether it is buried or remains on the surface, and the related cooling timescales. Comparing sandstone and limestone projectiles shows similar temperature and pressure profiles for the same impact velocities, with limestone providing slightly more favourable conditions for biomarker survival.

1. Introduction

The lunar surface has been impacted by a multitude of hypervelocity projectiles over its lifetime, leading to the heavily cratered surface we see today. This rich impact history is exemplified by the Late Heavy Bombardment (LHB), an epoch circa 3.9 Gyr ago when the terrestrial planets are postulated to have experienced frequent large-scale impact bombardment (Stöffler et al., 2006; Norman, 2009). Although it is still contentious whether or not the LHB occurred as a large spike of giant impacts at ~3.9 Ga (Turner et al., 1973; Tera et al., 1974; Cohen et al., 2000; Gomes et al., 2005), or as an initially very high impact rate which steadily decreased over time (Hartmann, 1975, 2003, 2019; Zellner, 2017), or as a hybrid of these possibilities (e.g., Turner, 1979; Marchi et al., 2012; Morbidell et al., 2012), it is undeniable that the early history of the Solar System was dominated by a higher rate of large impacts than today.

The epoch of enhanced impact rates may have extended well beyond 3.9 Ga ago on the Earth, with basin-forming impacts possibly continuing until about 2.5 Ga (e.g. Bottke et al., 2012; impact basins are impact structures >300 km in diameter). During this time, Earth would have experienced numerous, basin-forming, hypervelocity impacts (Marchi et al., 2014), potentially ejecting terrestrial material at velocities great enough to surpass escape velocity and take up Moon-crossing orbits (Armstrong et al., 2002; Beech et al., 2019). This has led to the proposal that such ejecta could be preserved on the lunar surface as terrestrial meteorites (Armstrong et al., 2002; Gutiérrez, 2002; Crawford et al., 2008; Armstrong, 2010). In particular, Armstrong (2010) showed that the transfer efficiency of Earth-escaping ejecta from large terrestrial

* Corresponding author.
E-mail address: shalim03@mail.bbk.ac.uk (S.H. Halim).

https://doi.org/10.1016/j.icarus.2020.114026
Received 30 January 2020; Received in revised form 22 July 2020; Accepted 31 July 2020
Available online 6 August 2020

impacts to the Moon was 10^{-5} to 10^{-4} and concluded that in some regions of the lunar surface, as much as 510 kg km^{-2} of terrestrial material may have impacted since 3.9 Ga. This equates to a globally averaged concentration of terrestrial material in the regolith between 36 and 61 kg km^{-2}. Even higher rates of delivery of terrestrial material to the Moon would be expected before 3.9 Ga owing to the higher rate of basin-forming impacts on the Earth. The recent discovery of a possible terrestrial clast in Apollo sample 14,321 by Bellucci et al. (2019) may provide physical evidence for terrestrial material surviving impact with the lunar surface, although this interpretation has now been questioned (Warren and Rubin, 2020).

The mass of solid terrestrial material that experiences low shock pressures yet is ejected at greater than Earth's escape velocity is a matter of debate. Theoretical estimates using extrapolation of an analytical model of spallation (Melosh, 1984; 1985) suggest that a mass of ejecta equivalent to as much as 10^{-5} to 10^{-2} of an impactor's mass may escape Earth's gravity without exceeding a shock pressure of 10 GPa (Armstrong et al., 2002). On the other hand, shock physics simulations of several Chicxulub-scale impact scenarios did not resolve any material ejected at escape velocity that was not shocked to the point capable of destroying entrained biomarkers (Artemieva and Morgan, 2009; Meyer et al., 2011). As these latter simulations employed a relatively coarse spatial resolution, and the results were only tabulated to fractions of $\sim10^{-3}$ of the initial impactor mass, they may not be incompatible with the estimates presented by Armstrong et al. (2002). In Section 3.1, we present new high-resolution 3D shock physics calculations that resolve the fraction of an impactor mass that is ejected with both high speed and low pressure, confirming that low-shock impact ejection from Earth to the Moon is possible, if inefficient.

Assuming that terrestrial crustal materials can survive launch from Earth and subsequent impact with the lunar surface, the lack of an atmosphere, hydrological cycle, or plate tectonics enhance the likelihood that the Moon might preserve a record of early Earth contained within terrestrial meteorites (Joy et al., 2016). These terrestrial meteorites could therefore provide a record of early biological evolution on Earth from a period that predates the earliest evidence of life on Earth itself. Suitable biological-markers (biomarkers) in such terrestrial meteorites would be complex molecular fossils derived from biochemicals of living organisms (Peters et al., 2004), and conceivably even microfossils of early organisms. Terrestrial meteorites ejected later in Earth's history might possibly contain macrofossils of various kinds, although these would be of less interest as the Earth's own geological record has retained a good record of more recent times.

Although the lack of a lunar atmosphere makes for a less than soft landing for incoming projectiles, the low gravity and escape velocity means that a fraction of incoming projectiles will strike at relativity low impact velocities. Work by Armstrong et al. (2002) and Armstrong (2010) estimated the maximum velocity of a terrestrial meteorite landing on the lunar surface at any time since 3.9 Ga ago would have been $\sim$5 km s^{-1}, and that >70% would impact with a vertical velocity component less than 2.5 km s^{-1} (owing to the high likelihood of oblique impacts). The fate of the projectile and survivability of organic material in impacts has been previously assessed by multiple studies. Rock projectile materials in numerically simulated hypervelocity impacts have been shown to survive impact with multiple simulated planetary bodies including Earth (Pierazzo and Melosh, 2000; Wells et al., 2003; Potter and Collins, 2013; Beech et al., 2019), the Moon (Bland et al., 2008; Yue et al., 2013), and Jupiter's moon Europa (Pierazzo and Chyba, 2002). Earlier numerical models also indicate that volatiles and organic material within projectiles may survive impact with the Moon (e.g. Crawford et al., 2008; Ong et al., 2010; Svetsov and Shuvalov, 2015). Projectiles in laboratory-scale experiments can survive hypervelocity impacts with multiple target materials (Daly and Schultz, 2015; Wickham-Eade et al., 2018), and organic constituents within such projectiles have also been shown to survive (Mimura and Toyama, 2005; Parnell et al., 2010; Meyer et al., 2011; Burchell et al., 2014a, 2014b, 2017). The median survival time for centimetre to meter scale rocky material on the surface of an airless body such as the Moon has been estimated to be between 40 and 80 Ma, with some surviving up to 300 Ma, depending on the material (Basilevsky et al., 2013, 2015). Examples of surviving asteroidal material (see Joy et al., 2016 for an overview) have been found in lunar samples from Apollo 11 (Goldstein et al., 1970; McKay et al., 1970; Quaid and Bunch, 1970), Apollo 12 (Wood et al., 1971; Zolensky et al., 1996; Joy et al., 2020), and Apollo 16 (Jolliff et al., 1993). Additionally, fragments of surviving material have been identified in lunar breccias, including a chondritic fragment found within lunar meteorite Pecora Escarpment 02007 (Day et al., 2006; Liu et al., 2009; Joy et al., 2012), and some younger Apollo 16 regolith breccias (Joy et al., 2012).

Previous modelling to assess the survival of terrestrial projectiles impacting the lunar surface was performed by Crawford et al. (2008) using the ANSYS AUTODYN software package. They considered 0.5 m wide, solid basalt and sandstone cubes as projectiles impacting an unconsolidated sand target layer at 2.5 km s^{-1} and 5 km s^{-1}, with impact angles between 20° and 90°. Here we build on this earlier work using the two-dimensional version of the multi-material, multi-rheology iSALE (impact-Simplified Arbitrary Lagrangian Eulerian) shock physics hydrocode (Amsden et al., 1980; Collins et al., 2004; Wünnemann et al., 2006). Previously, specific peak pressure thresholds were used as a proxy for survivability in a variety of materials, with peak temperature from shock heating assumed to correlate with peak pressure. Whilst shock heating may dominate for high speed impacts that occur on Earth (minimum impact velocity of 11.2 km s^{-1}; e.g., Melosh, 1989), at lower impact velocities (<10 km s^{-1}), such as those associated with terrestrial meteorites impacting the Moon, recent work as shown that heating by shear deformation rather than shock may play an important or even dominant role in raising temperatures within target materials (Quintana et al., 2015; Kurosawa and Genda, 2018). If this result also applies to the heating of impactor material, survivability of projectiles and their possible organic or hydrated mineral constituents would be less favourable than previously thought. Therefore, to fully understand and quantify 'survival' of a biomarker, we must consider both pressure and temperature, implying the need for a well understood strength model which can resolve both shock and shear heating.

In this work, we investigate the survival of biomarkers in projectiles impacting the lunar surface. Survival of a molecular biomarker is defined using the method described by Pierazzo and Chyba (1999), where survival is assessed via the thermal degradation of amino acids, adopting a form of the Arrhenius equation and thermal degradation parameters unique to each biomarker. Larger microfossil biomarkers are also considered using pressure and temperature survival thresholds based on their survival in metamorphosed Earth rocks for which the experienced peak pressures and temperatures have been determined (Section 2.4).

2. Methods

2.1. iSALE modelling ejection of terrestrial material from Earth

We used the iSALE-3D shock physics code (Elbeshausen et al., 2009; Elbeshausen and Wünnemann, 2011) to simulate the high-speed ejection of terrestrial material via a basin-forming impact on Earth. We simulated a 50 km diameter projectile striking Earth at an angle of 45° to the surface and a speed of 20 km s^{-1}. This impactor size is representative of basin-forming impacts on the Moon and sufficiently large (greater than Earth's atmospheric scale height) that the influence of the atmosphere on the impactor and high-speed ejecta can be neglected. Both the impact velocity and angle of impact are the most common values for impacts on Earth (Shoemaker, 1962; Le Feuvre and Wieczorek, 2011). A current limitation of iSALE3D requires both the impactor and target to be the same material, therefore, we used a granite equation of state table for both impactor and target, which was made using the analytical equation of state package (ANEOS; Thompson and Lauson, 1972) with

input parameters derived by Pierazzo et al. (1997). The strength of the material was modelled using the method described by Collins et al. (2004) with identical parameters to those used to represent the impactor and crust in recent iSALE3D simulations of the Chicxulub impact (Collins et al., 2020). Launch speed and peak pressure of ejecta were recorded by tracer particles, which were then analysed to measure the cumulative mass of material that was ejected from the target at speeds faster than ejection velocity (11.2 km s^{-1}) yet at the same time experienced pressures lower than those required to melt the material. The simulations were run long enough to measure all ejecta launched faster than ~5 km s^{-1}. A series of simulations of the same impact scenario but with different spatial resolutions, from 40 to 100 cells per projectile radius (cppr), was performed to test the robustness of the results.

2.2. iSALE modelling of terrestrial meteorite impacts on the Moon

Building upon previous modelling studies (Armstrong et al., 2002; Armstrong, 2010; Crawford et al., 2008), we used the iSALE-2D shock physics code (Wünnemann et al., 2006) to simulate vertical impacts of terrestrial meteorites into the lunar surface. Our modelling approach followed previous projectile survivability studies using iSALE and other shock physics codes (e.g., Pierazzo and Melosh, 2000; Crawford et al., 2008; Davison et al., 2011; Potter and Collins, 2013), but considered impact scenarios relevant for impact of terrestrial meteorites on the Moon. Here we describe the justification for our choice of input parameters. For more details about the modelling approach, including diagnosis of shock pressures and temperatures (Section S1), scenario descriptions (Table S1), and choice of resolution (Fig. S1), please refer to the online supplement.

Terrestrial meteorites were modelled as 0.5 m diameter, sandstone, and limestone projectiles, vertically impacting a basalt target at 2.5 and 5 km s^{-1}. Projectile shape was varied between a sphere, oblate spheroid, and prolate spheroid. The two impact speeds considered in this work, 5 and 2.5 km s^{-1}, represent the highest impact speed as well as the most likely impact speed of terrestrial meteorites striking the lunar surface, estimated by Armstrong et al., 2002 and Armstrong, 2010. Oblique impacts were not considered here; the effects of changing the angle of impact on the fate of the impactor have been well-documented by previous research (e.g., Pierazzo and Melosh, 2000; Crawford et al., 2008; Davison et al., 2011; Potter and Collins, 2013), showing that the more oblique the impact, the lower the pressures experienced by the projectile. The vertical impact simulations presented here therefore represent a conservative estimate of surviving material at a given impact speed.

To investigate a range of possible sedimentary projectile materials and target types, porosity was varied in both the projectile and the target layer (Table S1). The basis for a 30% target porosity stems from Apollo samples with intra-granular porosities in lunar regolith of 21–32%, rising to 52% when including inter-granular porosities (Carrier et al., 1991). An upper limit of 70% porosity was chosen based on the results of the Lunar Crater Observation and Sensing Satellite (LCROSS) impact which suggested a surface porosity of >70% in Cabeus crater (Schultz et al., 2010); interestingly, Cabeus is geographically located in a region where terrestrial meteorites may be relatively common according to direct transfer models of terrestrial material to the Moon during giant impacts (Armstrong, 2010).

The solid components of the impactor and regolith were modelled using equation of state tables derived from the analytical equation of state package (ANEOS; Thompson and Lauson, 1972) with input parameters for quartz (sandstone; Melosh, 2007), calcite (limestone; Pierazzo et al., 1998) and basalt (lunar surface; Pierazzo et al., 2005), respectively. The maximum shock pressure in the projectile in our simulations ranged from 9 to 63 GPa, depending on projectile speed and target and material properties. This range coincides with the assumed pressure of the solid-solid phase transition in quartz (21 GPa) employed in the ANEOS equation of state (Melosh, 2007). As a consequence, a small volume of projectile material along the symmetry axis, in some impact scenarios, was driven into the mixed-phase state across the transition, which resulted in spuriously high temperatures recorded for this material. The quartz equation of state table was, therefore, modified for this specific study to remove the solid-solid phase transition, so that the high-pressure phase of quartz was not represented. While this removed the spurious temperatures within the projectile, the absence of any phase transition implies that temperatures associated with pressures exceeding ~20 GPa in this work are overestimated within the projectile material and therefore any conclusions made regarding biomarker survival should be deemed as conservative estimates.

The strength of the sandstone (projectile), limestone (projectile) and basalt (target) materials was modelled using the method described by Collins et al. (2004), with parameters for a weak granular material. Inclusion of a strength model for the projectile material allows us to explicitly resolve heating of materials via both shock and shear processes. Parameters for the Collins strength model were taken from those used previously for a limestone material in a terrestrial impact simulation by Goldin et al. (2006). All of the limestone simulations used a spherical projectile shape model and the same porosity model parameters as those used in the sandstone projectiles.

Peak-shock pressures and temperatures were extracted from the simulations using the tracers placed within the projectile. Results were collected until the point where the rarefaction wave had passed through the projectile and travelled into the target, after which peak pressures and temperatures were observed to stop increasing. Post-shock temperatures were extracted from the tracers once the projectile had been released from the high-pressure regime.

2.3. Material strength and shear heating in the projectile

During high-velocity impacts, some of the initial kinetic energy of the projectile is converted into internal energy (heat) of the projectile due to its sudden compression. For sufficiently high impact speeds the projectile material is heated dramatically at the point of contact and can melt or vaporise upon release from high pressure. Another heating mechanism during impact is the conversion of distortional energy to internal energy, known as shear heating, which has been largely overlooked in the history of numerical impact modelling (Kurosawa and Genda, 2018; Melosh and Ivanov, 2018). In high (>15 km s^{-1}) velocity impacts, the mass of material heated by shock heating exceeds the mass heated via shear heating and can reasonably be neglected. However, Quintana et al. (2015) identified that material strength is important for low-velocity impacts, increasing melt and vapor generation, and Kurosawa and Genda (2018) concluded that additional shear heating was significant for impacts with velocities below 10 km s^{-1}. The additional heat reduced the impact-velocity thresholds for the onset of melting from 8 and 10 km s^{-1} in strengthless rocks to 2 and 6 km s^{-1} when including strength, respectively.

Whilst Kurosawa and Genda (2018) considered the effect of shear heating in the target, its importance in projectile survivability has not been addressed as most previous studies of the fate of the projectile have assumed a strengthless impactor (e.g., Pierazzo and Melosh, 2000; Crawford et al., 2008; Potter and Collins, 2013). Here we quantify the influence of shear heating within this projectile material by comparing identical simulation scenarios with and without a strength model. We simulated a solid, spherical projectile impacting a solid target at 2.5 and 5 km s^{-1} to investigate the variation in shear heating at differing velocities. The same model parameters were used as described in Section 2.2, with the exclusion of the strength model in one set of simulations at both 2.5 and 5 km s^{-1}.

2.4. Biomarker selection

To quantify the survival of biomarkers within terrestrial meteorites, we identified a set of organic materials that may be contained within terrestrial rocks and that could potentially survive impact with the lunar

surface once ejected from Earth. The organic materials chosen include examples of four amino acids and the molecule lignin (Table 1), where the latter is important in the formation of cell walls (Brebu and Vasile, 2010). Following the method described by Pierazzo and Chyba (1999), biomarker survivability as a function of temperature was estimated using a modified version of the Arrhenius equation (Nelson, 1967):

$$dM = -MAe^{-\frac{E_a}{RT(t)}}dt \quad (1)$$

where:

M = mass of organic material (kg).
A = pre-exponential factor (s^{-1}).
E_a = activation energy of organic molecule (kcal mol1).
R = gas constant (kcal K^{-1} mol^{-1}).
T(t) = time dependant temperature (K).
dt = change in time (s).

Amino acid and lignin thermal decomposition is assumed to occur by a single reaction of the first order for their respective A and E_a values. This means the reaction proceeds at a rate that depends linearly on only one reactant concentration. Amino acids with alkyl groups (e.g. valine) can survive pressures up to ~28 GPa, with 1–4% of the initial mass of amino acid surviving, and much larger percentages (up to 70%) beneath ~21 GPa (Bertrand, 2009).

Cooling timescales for surviving projectile fragments can be bracketed by two end-member scenarios representing the slowest and fastest cooling times that can be realistically expected. The slowest cooling rate assumes the projectile survives impact as an unbroken sphere and is buried entirely in the insulating lunar regolith, thereby undergoing slow, conductive cooling. The fastest cooling rate refers to a smaller fragment which is ejected, lands on the surface regolith, and undergoes fast, radiative cooling to space. Regolith properties (including density, specific heat capacity, and thermal conductivity) were taken from Fagents et al. (2010) and combined with temperature data from our models to calculate the conductive heat transfer from projectile to regolith; we assumed steady state heat conductivity and cooling of an isothermal sphere buried in a medium of known temperature (Lienhard and Lienhard, 2001). For radiative cooling, the equation for radiative cooling of an idealised sphere was used (Nave, 2017).

Table 2 shows examples of larger biomarkers in the form of microfossils and small fossilised remains. Using the thermal degradation method is not valid for these examples as they are composed of multiple molecules and therefore too complex to be estimated by the first-order approximation of the Arrhenius equation. Instead, the fossils have been chosen due to their survival in low-grade metamorphosed rocks (of known P-T conditions) for which the experienced peak pressures and temperatures have been determined (Bernard et al., 2007; Laborda-López et al., 2015; Shaw, 2019). It is important to note that these are not the maximum survival pressures and temperatures for each fossil itself, but the estimated maximum pressures and temperatures experienced by fossils shown to have survived. The maximum pressure experienced by the 300 μm lycophyte megaspores was constrained by the maximum silica content of phengites within the limestone sample (which had undergone metamorphism in the blueschist facies), used as a quantitative proxy to estimate peak pressure (Bernard et al., 2007). Peak temperature (630 K) was constrained by the Fe-Mg exchange between Mg-carpholite and chloritoid, further supported by Raman spectroscopy of carbonaceous material (~633 K; Bernard et al., 2007). Ammonites were found in a hornfels sample which experienced a minimum temperature of 800 K, estimated from the transition of pyrite to pyrrhotite and pressures of 0.02 GPa based on the depth of burial and density of materials above at the time of metamorphism (Shaw, 2019). Crinoids and some examples of cephalopods, among other fossil assemblages, were found in alpine marble and calc-silicate schist samples which survived temperatures of ~750 K and pressures ~0.2 GPa (Laborda-López et al., 2015). Whilst we are not expecting to find macroscopic fossils such as ammonites and crinoids in 3.9 Gyr Earth rocks, we use these macrofossils as examples of fossil survivability as a comparison to the molecular biomarkers.

Table 1
Examples of organic materials that may be contained within terrestrial rocks, with thermal degradation parameters and decomposition/vaporisation temperatures based upon published experimental results.

Biomarker	Thermal degradation parameters	Reference
Arginine	A = 134 s^{-1} E_a = 8.79 kcal mol^{-1}	Rodante, 1992
Valine	A = 49 s^{-1} E_a = 6.7 kcal mol^{-1}	Rodante, 1992
Glutamine	A = 14.9 s^{-1} E_a = 5.9 kcal mol^{-1}	Rodante, 1992
Tryptophan	A = 8.2 s^{-1} E_a = 6.2 kcal mol^{-1}	Rodante, 1992
Lignin	A = 2.82 s^{-1} E_a = 6.0 kcal mol^{-1}	Brebu and Vasile, 2010

3. Results

3.1. Ejection of material from Earth to the Moon

Results from the 3D simulations confirm that, in a typical large impact on Earth, some solid ejecta can transfer to the Moon. In the highest resolution simulation (100 cppr), the total mass of material ejected faster than escape velocity (M_{ej} > 11.2 km s^{-1}) is 5.5 × 10^{-2} impactor masses (M_i) (Fig. 1). Ejected material that can still be considered solid (i.e., terrestrial meteorites that experience pressures lower than a nominal critical pressure for melting of 50 GPa) amounts to a mass fraction of 1.3 × 10^{-3} M_i. Given the very different methods used to determine the mass of escaping solid ejecta, our estimate derived from high-resolution simulation of oblique impact is remarkably similar to estimates made by Armstrong et al. (2002) for a vertical impact at a similar impact speed (see their Table V), which used analytical ejecta mass-velocity scaling relationships (Melosh, 1985). Our results therefore broadly support their predictions of the efficiency of Earth-Moon transfer. Armstrong (2010) showed that direct transfer of ejecta from Earth to the Moon, which requires ejection speeds between ~10.9 and 11.2 km s^{-1} to place the ejecta in lunar orbit, was the most efficient transfer mechanism at (and prior to) 3.9 Ga, with an efficiency of ~1 × 10^{-4}. According to our simulation, a total ejecta mass (all shock levels) of approximately 4 × 10^{-3} M_i and a solid ejecta mass of approximately 3 × 10^{-4} M_i is ejected at speeds within this range. This suggests that the mass flux of terrestrial material to the Moon was approximately 4 × 10^{-7} times the mass flux of large impactors striking Earth during the LHB, consistent with previous estimates (Armstrong et al., 2002; Armstrong, 2010). As the Moon recedes from Earth, the minimum ejection speed required to reach lunar orbit increases and hence the efficiency of direct transfer diminishes. However, ejecta that leave the Earth-Moon system (launched faster than escape velocity) can also subsequently strike the Moon via "orbital transfer" or "lucky shots", which have comparable efficiencies of 4 × 10^{-5} (Armstrong et al., 2002). Thus, a lower bound on the mass of terrestrial meteorites striking the Moon since 3.9 Ga is ~5 × 10^{-8} times the mass of large impactors striking Earth. We note that the mass of terrestrial material reaching the Moon prior to 3.9 Ga would have been higher because of both a higher flux of large impactors striking Earth and a higher transfer efficiency from Earth to the Moon due to the Moon being closer to the Earth.

Fig. 1 also shows that high spatial resolution is necessary to resolve the low-shock, high velocity escaping ejecta. While the mass of solid escaping ejecta is well resolved at 100 cppr, simulations with a resolution of 40 cppr are unable to resolve any solid escaping ejecta. This explains the discrepancy between our high-resolution simulation results and the results of low(er) resolution simulations of the Chicxulub impact (Artemieva and Morgan, 2009). Low-shock material ejected fast enough

Table 2
Fossil and microfossil biomarkers that may be contained within terrestrial rocks with minimum survival pressures and temperatures based upon examples found in metamorphosed Earth rock samples.

Biomarker	Rock type	Minimum survival conditions based upon metamorphosed samples		Reference
		Pressure (GPa)	Temperature (K)	
Ammonites	Hornfels	0.02	800	Shaw, 2019
Crinoids/Cephalopods	Graphitic marble and calc-silicate schist	0.2	750	Laborda-López et al., 2015
Lycophyte megaspores	Limestone – blueschist facies	1.4	630	Bernard et al., 2007

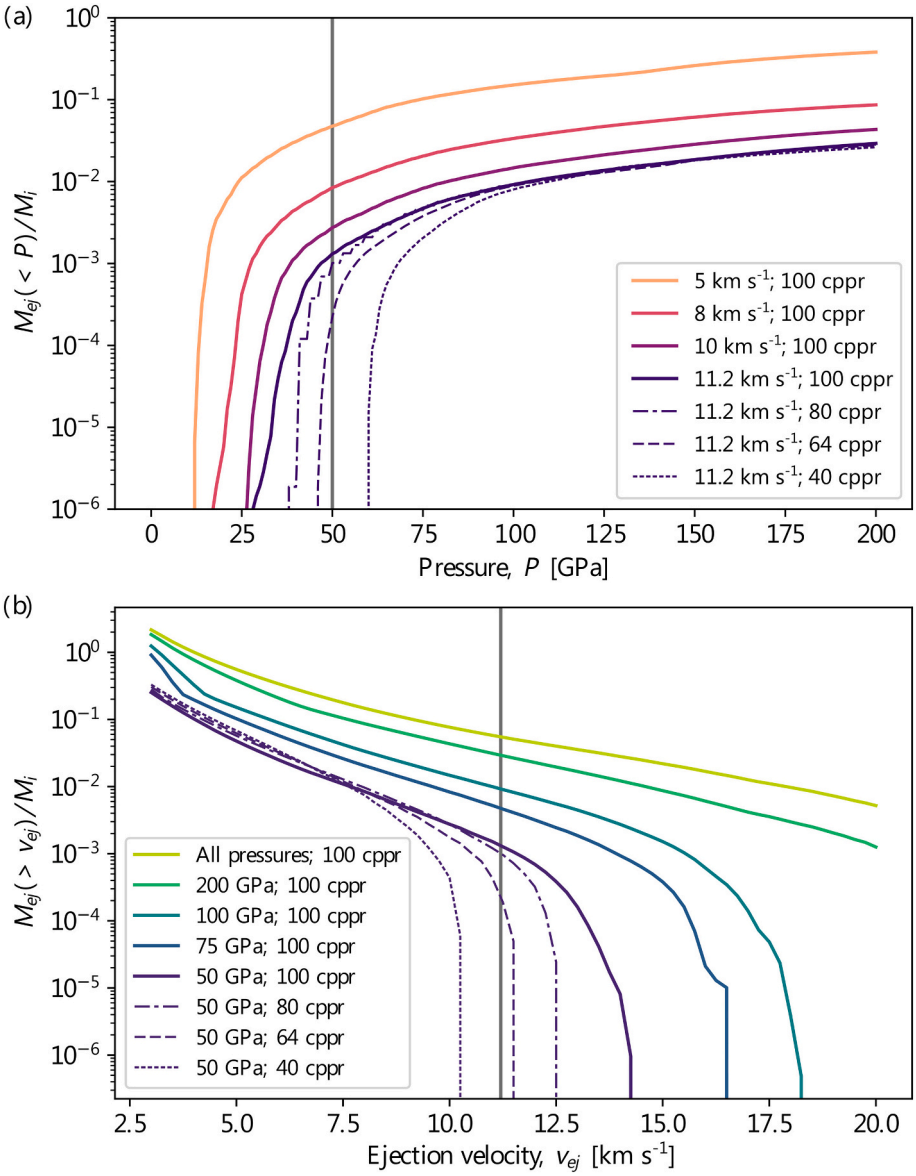

Fig. 1. The cumulative mass of target material ejected (M_{ej}) as fraction of impactor mass (M_i) shown as a function of shock pressure for different ejection speeds (a) and as a function of ejection speed for different shock levels (b). The influence of spatial resolution is shown for the solid ejecta ($P < 50$ GPa) that escapes Earth ($v_{ej} > 11.2$ km s^{-1}).

to escape Earth originates from very close to the surface of the target, in close proximity to the impact site (Fig. 2). This is the so-called interference zone where interaction between the shock and release waves generates very steep pressure gradients but shields the ejected material from high pressure (Melosh, 1984). The minimum shock pressure experienced by ejected meteorites in the 100 cppr (250 m cell size) simulation is ~30 GPa, however even at this high resolution the simulation is not fully resolved at the lowest shock pressures (Fig. 1a) and the cell size is much larger than expected size of individual meteorites. It is therefore likely that a small volume of even lower shock ejecta, not resolved in our simulations, will be transferred to the Moon.

3.2. Survivability of terrestrial meteorites impacting the Moon

3.2.1. The influence of material strength

The results of our meteorite survivability simulations show that at

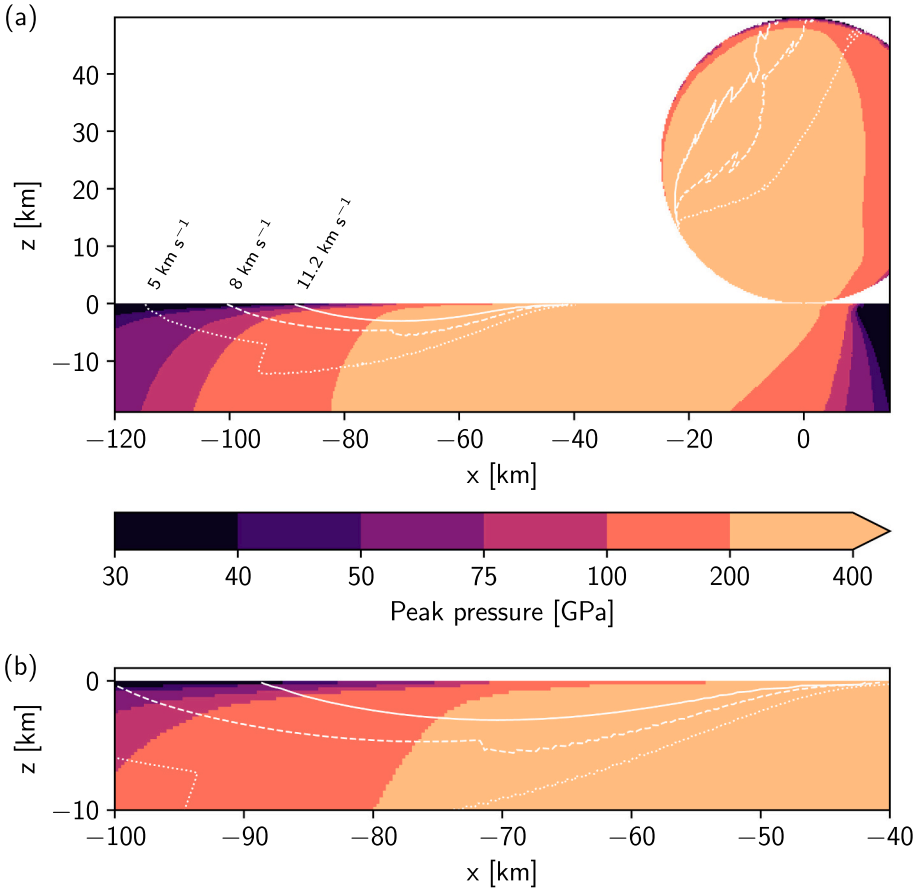

Fig. 2. Provenance plot of high-speed ejecta that experiences different peak shock pressures for a simulation of a 50-km diameter impactor striking Earth at 45° to the surface and with a speed of 20 km s^{-1} with resolution 100 cppr. The spallation zone from (a) is highlighted in (b). The direction of impact is from right to left. White contour lines display ejection velocity.

impact speeds of both 2.5 km s^{-1} and 5 km s^{-1} peak-shock temperatures are significantly higher across most of the projectile when projectile strength is accounted for, whilst peak pressure is almost unaffected (Fig. 3). This is consistent with previous work that investigated shear heating in target materials (Quintana et al., 2015; Kurosawa and Genda, 2018). Peak-shock pressures in the projectiles were approximately the same for the spherical projectile impacting a solid target at 2.5 and 5 km s^{-1}, with and without strength in the projectile. However, there is a marked difference in the peak temperatures experienced for the with strength vs. strengthless projectile in both the 2.5 km s^{-1} and 5 km s^{-1} scenarios (Fig. 3). At 2.5 km s^{-1}, in the simulations with no strength, over 90% of the projectile volume experienced peak temperatures less than 400 K, whilst in the scenario with strength only 10% of the projectile experienced temperatures less than 400 K. At 5 km s^{-1}, a similar pattern was observed where over 90% of the strengthless projectile experienced temperatures less than 900 K, while the only 15% of the projectile with strength experienced temperatures less than 900 K. The inclusion of both shear and shock heating is therefore crucial in considering the temperatures experienced by terrestrial meteorites striking the Moon at velocities less than 5 km s^{-1}.

3.2.2. *Influence of impactor velocity, shape, porosity, and composition*

Our simulations demonstrate that terrestrial meteorites striking the Moon can experience large range of pressures and temperatures, depending on the impactor speed, composition, porosity, and shape, as well as the nature of the impacted target surface. For a full description of these results, please refer to the supplementary material (Section S2). Table 3 provides a summary of the mean pressure and temperatures recorded for each projectile in all of the scenarios considered. Increasing the speed of the projectile increases the peak pressures and temperatures experienced by the projectile (Fig. S2), as expected. Mean peak pressure and temperature are reduced with increasing porosity of the target for both impact speeds considered (Fig. S3), whilst increasing porosity in the projectile produces a slight decrease in mean peak pressure, but a marked increase in peak temperature (Fig. S4). For the same impact speed, prolate projectiles experience lower pressures than their spherical counterparts, but higher temperatures (Fig. S5). Oblate projectiles experience the opposite trend (Fig. S6).

For the sandstone projectiles, Figs. 4 and 5 show the extremes of peak-shock pressure and temperature for the most and least favourable scenarios for biomarker survival in the simulation results, respectively. Pressure and temperature variations across the projectile are displayed using the information recorded by tracers in the projectile, mapped onto the original shape of the projectile. Any temperatures that display values less than 200 K (darkest blue in post-shock temperature plots of Figs. 4 and 5) should be ignored as these represent tracers in material which has either gone into tension and become unphysical or has left the simulation boundaries via ejection. Fig. 4 shows the result of a solid projectile impacting a 70% porous target at 2.5 km s^{-1}. Temperatures across the majority of the projectile do not exceed 600 K and remain at these temperatures for the duration of the simulation. Fig. 5 shows the least favourable conditions for biomarker survival. In this case, peak temperatures exceed 2000 K and would prevent any substantial proportion of biomarker to survive across most of the projectile. However, post-shock temperatures decrease to less than 800 K away from the projectile centre, as can be seen in the post-shock tracer plot in Fig. 5. This rapid decrease in temperature for a fraction of the projectile material over the course of the relatively short simulation time (0.005 s) bodes

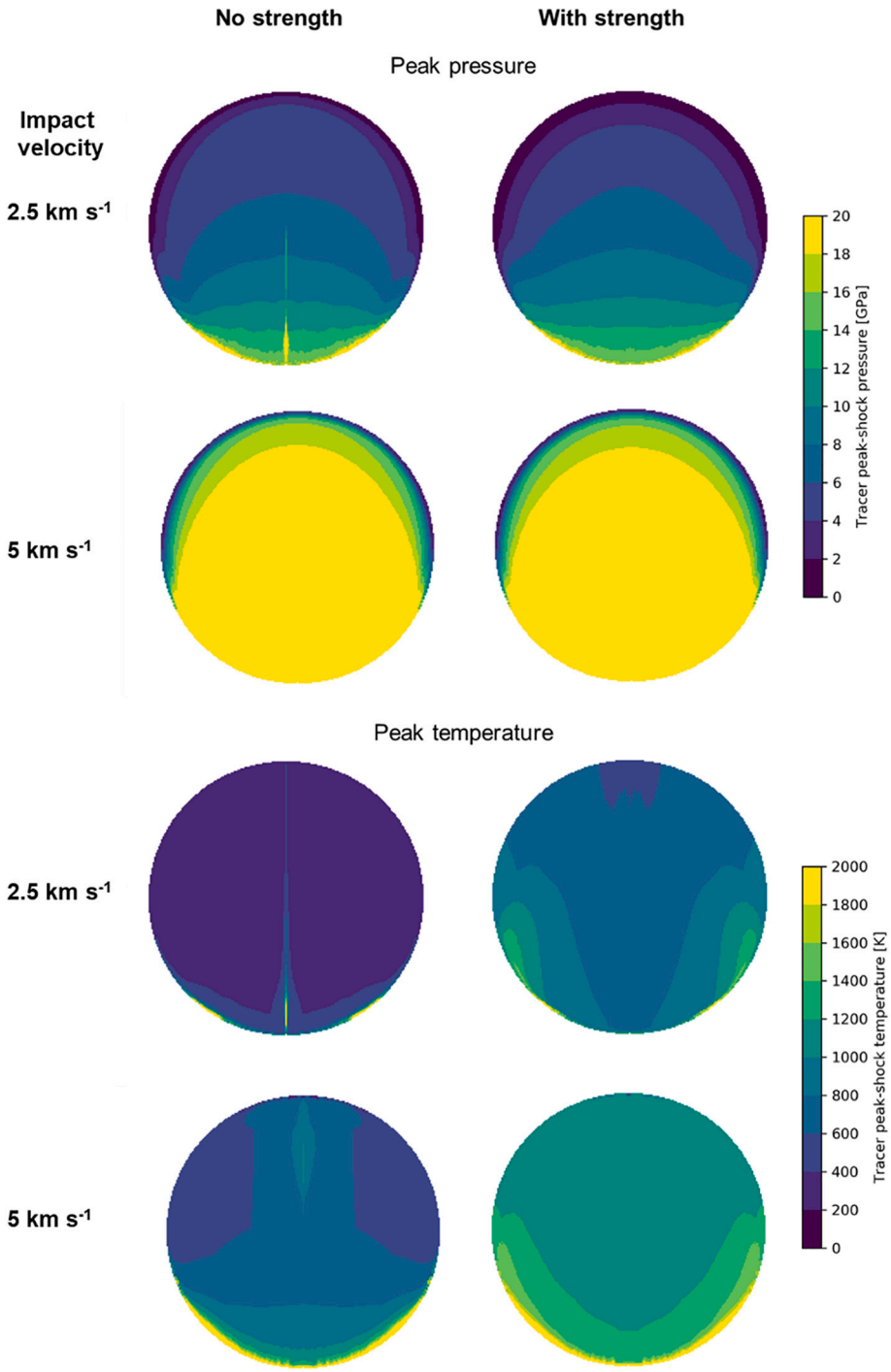

Fig. 3. Contour maps of peak pressure (top) and temperature (bottom) for solid projectiles impacting a solid target at 2.5 km s^{-1} and 5 km s^{-1}. Left projectile maps used no strength model (hydrodynamic), right projectile maps used a rock strength model (Collins et al., 2004) which could explicitly resolve shock and shear heating. Projectile maps in this and all figures going forward show the state of the projectile volume mapped onto the original shape of the projectile before impact; it is not a representation of the final shape or distribution of the projectile mass.

well for biomarker survival.

Peak-shock pressures in the limestone projectiles were almost identical to those in the sandstone projectiles across all the simulations (Table S2). However, peak, and post-shock temperatures were both reduced in the limestone projectiles relative to the sandstone projectiles, with the most noticeable difference in solid projectiles impacting solid targets at 2.5 km s^{-1} (Table 3 and Fig. 4). The potential survivability of biomarkers is more favourable in the limestone projectiles shown in Fig. 4 as temperatures are lower in the rear portion of the projectile by ~200 K, i.e. reduced from a maximum of 600 K to 400 K. This peak-temperature reduction translates to post-shock temperature, recorded at the final timestep (5 ms), with the surviving material experiencing maximum temperatures of 600 K across most of the projectile. This represents the most favourable conditions for biomarker survival. In the least favourable scenario for biomarker survival (Fig. 5), peak-shock temperatures reach 2000 K and higher, however, the material temperatures have reduced below 1600 K by the time that post-shock temperatures are recorded (5 ms). Overall, across each of the limestone scenarios, the results show that the fraction of material in which biomarkers could potentially survive is increased compared to sandstone projectiles.

Whilst peak pressures for relevant models in this study are comparable with those obtained in previous work (Crawford et al., 2008), the peak temperatures are higher than those predicted for strengthless

Table 3
Mean peak pressure and temperature results for each of the simulation scenarios. The names given to the simulations indicate the material of the projectile, the extent to which the projectile and target are porous, and the impact velocity. For example, "S_30_0_5" represents a sandstone projectile (S), with 30% porosity (30), impacting a solid (0) target at 5 km s^{-1} (5). Oblate and prolate scenarios feature solid, sandstone projectiles into a solid target.

Simulation ID (2.5 km s^{-1})	Mean peak pressure (GPa)	Mean peak temperature (K)	Simulation ID (5 km s^{-1})	Mean peak pressure (GPa)	Mean peak temperature (K)
S_0_0_2.5	6.08	830	S_0_0_5	23.4	1210
S_0_30_2.5	4.24	745	S_0_30_5	16.2	1100
S_0_50_2.5	2.80	630	S_0_50_5	12.3	1050
S_0_70_2.5	1.67	485	S_0_70_5	7.27	990
S_10_0_2.5	6.55	895	S_10_0_5	21.9	1400
S_20_0_2.5	6.55	1015	S_20_0_5	20.6	1640
S_30_0_2.5	6.29	1150	S_30_0_5	19.3	1950
S_40_0_2.5	5.73	1290	S_40_0_5	18.1	2370
Prolate_2.5	2.45	1050	Prolate_5	8.56	1330
Oblate_2.5	14.7	565	Oblate_5	43.8	1200
L_0_0_2.5	6.62	660	L_0_0_5	23.5	1035
L_0_70_2.5	1.82	480	L_40_0_5	18.4	2290

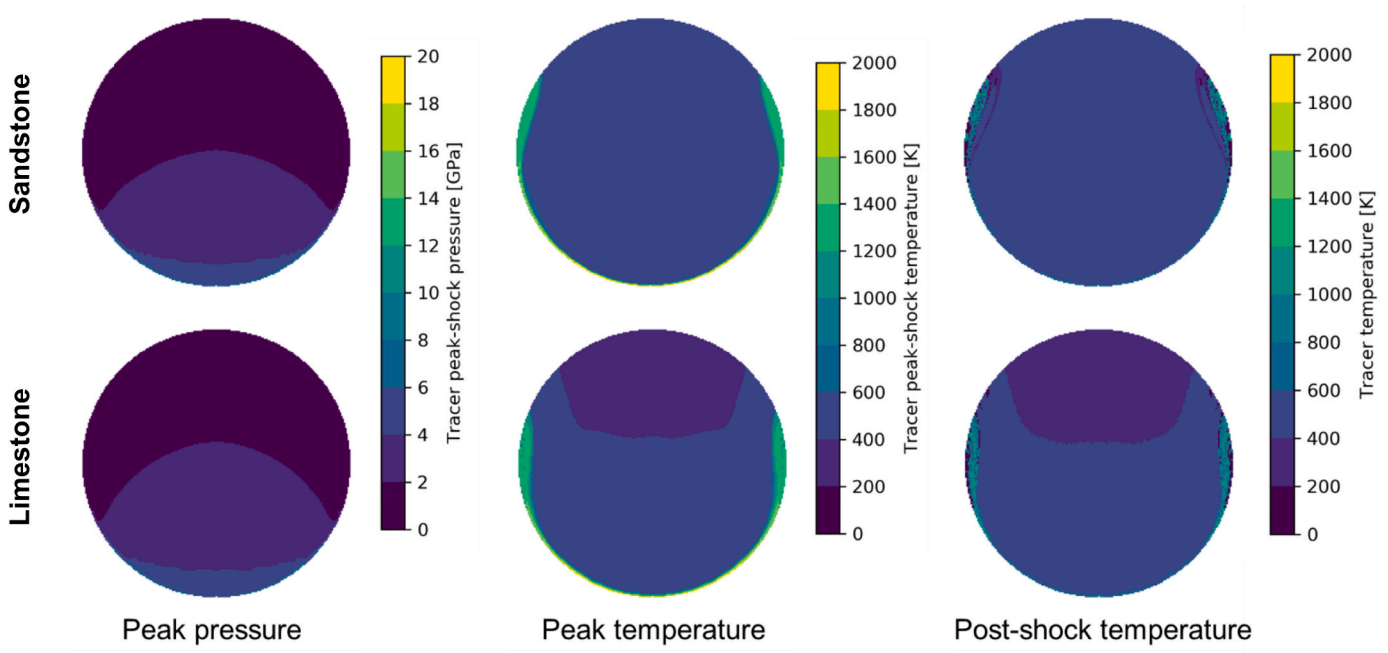

Fig. 4. Contour plots of comparing pressure and temperature regimes in sandstone (top) and limestone (bottom) projectiles. Both sets of plots are the result of a solid projectile impacting a 70% porous target at 2.5 km s^{-1} (most favourable for biomarker survival).

material based on peak pressures alone owing to the effect of shear heating (Kurosawa and Genda, 2018). As a result, the peak-shock temperatures are higher than expected across all of the simulations compared to those predicted by shock heating alone. Peak-shock temperatures are observed to decrease with increasing target porosity and increase significantly with increasing projectile porosity, emphasising the need to consider both pressure and temperature in the assessment of biomarker survivability. Therefore, compared with previous work we find less favourable conditions for survivability of the projectile, especially for projectiles travelling at the maximum expected impact velocity of 5 km s^{-1} (Armstrong et al., 2002; Armstrong, 2010). For otherwise identical simulations with an impact speed of 2.5 km s^{-1}, temperatures in the projectiles are much more favourable, experiencing temperatures that are on average ~500 K less than their 5 km s^{-1} counterparts. The potential for survival of all of the example organic molecules in terrestrial impactors is greatly increased for the lower velocity scenarios (i.e., 2.5 km s^{-1}), which would account for >70% of the terrestrial projectiles impacting the lunar surface at 3.9 Ga ago (Armstrong et al., 2002).

3.2.3. *Sandstone projectiles – molecule biomarker survival*

In order to gauge biomarker survival beyond immediately post-impact, it is necessary to consider biomarker survival in the projectile fragments because, although the temperatures within the projectile fragments will only decrease with time, they may remain elevated for a sufficient time for biomarker degradation to occur. We use the post-shock temperatures taken from the final timestep of the simulations as the starting temperature and estimate the cooling of the projectile material over 100 s (methods detailed in Section 2.4). We ignore the brief period of time during compression and release when the projectile experiences peak temperatures and then rapidly cools to the post-shock temperatures, as the effect on biomarker survival is minimal (<0.05% reduction in mass). From these calculations, a sphere with diameter 0.5 m (representing the unbroken projectile) and initial temperature 1000 K will radiatively cool to 900 K in ~100 s and conductively cool to 900 K in ~4 days. This example demonstrates the importance of considering both the temperature of the surviving projectile (fragmented or otherwise), and also the location in which the material is cooling, as biomarkers will degrade much more significantly under prolonged elevated temperatures. Post-impact biomarker survival was conservatively estimated based on the degree of thermal degradation, calculated using the Arrhenius equation (Section 2.4). The assumption that the projectile remains unfragmented and completely buried in the regolith is

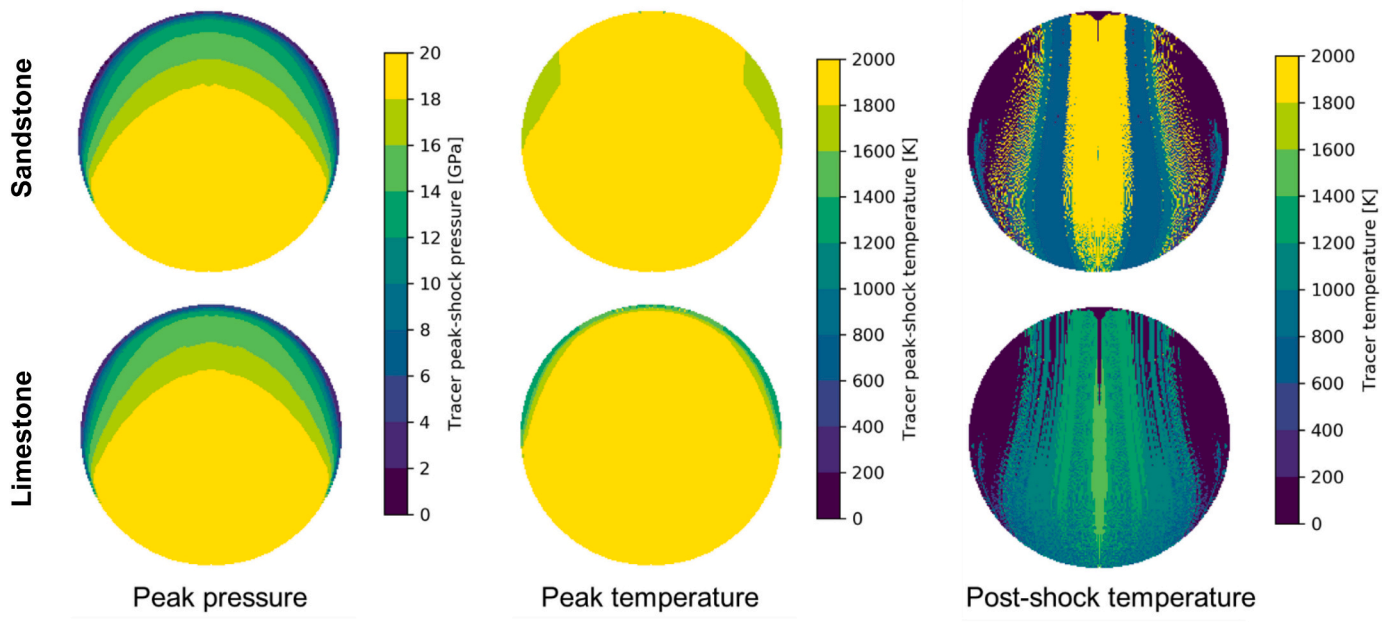

Fig. 5. Contour plots of comparing pressure and temperature regimes in sandstone (top) and limestone (bottom) projectiles. Both sets of plots are the result of a 40% porous projectile impacting a solid target at 5 km s^{-1} (least favourable for biomarker survival).

unreasonable based on the deformation seen in our simulations. Therefore, we approximate a fragment of ejecta as a 1 cm diameter sphere to compare the biomarker survival between radiatively cooling at the surface and conductively cooling whilst buried in regolith. Based upon these cooling timescale calculations, we can determine the best and worse-case scenarios for surviving biomarkers in the simulated projectiles (Figs. 6–8). It is important to note that the actual size of terrestrial meteorites will not greatly influence the peak or post-shock temperatures experienced upon impact, however the cooling rates do heavily depend upon the size of the surviving material.

The most favourable impact conditions for biomarker survival (illustrated in Fig. 4) are combined with the most favourable (radiative) and least favourable (conductive) projectile cooling conditions in Fig. 6a and b, respectively. All of the biomarkers survive in significant quantities in the best-case scenario (Fig. 6a), with lignin, tryptophan and arginine having the highest surviving fractions after 100 s (69%, 41%, and 33% respectively). These fractions are likely to stay constant over time as the rate at which the biomarker is degrading after 100 s has plateaued. However, in the least-favourable projectile cooling conditions (Fig. 6b) we see that valine, glutamine and arginine have degraded to values less than 0.1%, with lignin and tryptophan rapidly degrading at a constant rate after 100 s of cooling. Results illustrated in Figs. 6b, 7b, and 8b confirm that it is highly unlikely that the selected biomarkers will survive across any of the simulated impact conditions when subjected to conductive cooling times associated with burial in an insulating regolith. On the other hand, fractions of both lignin and tryptophan are shown to survive in the least favourable impact scenario simulated (Fig. 5), especially if concentrated in an area away from the centre of the projectile (Fig. 7a). Comparing the surviving percentage of a biomarker away from the centre of the projectile with one at the centre leads to a decrease from 42% to 7% for lignin and 12% to 0.1% for tryptophan (Figs. 7a and 8a).

Although largely neglected by previous studies regarding post-impact biomarker survival, the cooling timescales of surviving projectile fragments are important when considering the long-term thermal degradation of organic material. Even if the impact simulations imply pressures and temperatures compatible with the survival of significant proportions of organics immediately after the impact, depending on where the projectile fragments end up, and the size of the fragments, the cooling timescales to reach temperatures consistent with long-term survival may be on the order of days or weeks.

3.2.4. *Sandstone projectiles - fossil biomarker survival*

All of the molecule biomarkers will survive to some degree in at least one of the impact scenarios, however, this is not the case for the conservative estimates of the fossil ammonite, crinoid, and cephalopod survival. For the sandstone projectiles, peak temperatures in six of the 2.5 km s^{-1} velocity impacts and two of the 5 km s^{-1} impacts are below the threshold for survival of ammonites, crinoids and cephalopods (Table 2), in at least part of the projectile. However, pressures in every permutation of simulation were too great for any significant proportion of the ammonite, crinoid and cephalopod fractions to survive, even in the most favourable conditions (Fig. 4). The conservative survival pressure estimates taken from metamorphosed ammonite and crinoid/cephalopod samples of 0.2 GPa and 0.02 GPa respectively, are too low for identifiable fragments to survive hypervelocity impacts, even when impacting highly porous, unconsolidated surfaces. Lycophyte megaspores have a higher-pressure threshold for survival, according to preservation in terrestrial metamorphic samples (Tables 2, 1.4 GPa). All impacts with velocities of 5 km s^{-1} produced peak pressures across the projectile greater than the pressure threshold, whilst any projectiles that included porosity produced temperatures greater than the temperature threshold. Oblate and prolate projectiles also exceeded the pressure and temperature thresholds, respectively. Finally, we consider scenarios with impact velocities of 2.5 km s^{-1}, with solid projectiles impacting targets of varying porosity (Fig. 9). Peak pressure and temperature regimes within these particular projectiles are favourable for the survival of lycophyte megaspores, with varying fractions of the projectiles being conducive to survival in each scenario. Increasing the porosity of the target has previously been shown to decrease both pressure and temperature across the impacting projectile. Therefore, in the scenarios shown in Fig. 9, lycophyte megaspores would be expected to survive in a greater proportion of the projectile for increasing target porosity, especially towards the back of the projectile where pressures and temperatures are not as extreme. Note that in this case, consideration of cooling timescales of the post-impact projectile fragments can be neglected, as the survival temperatures are taken from samples which have undergone progressive heating and cooling over millions of years.

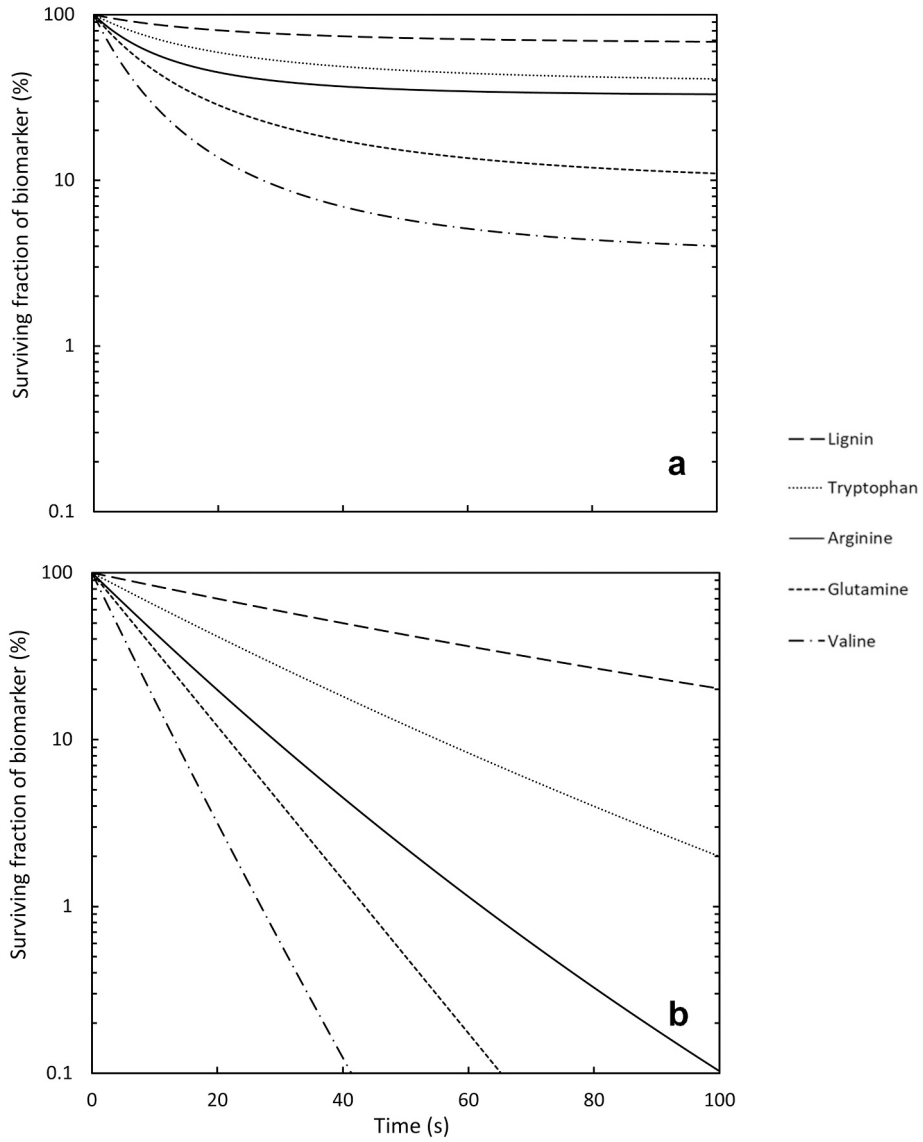

Fig. 6. Survival of selected biomarkers for a tracer that reaches a post-shock temperature of 600 K in the main body of the sandstone projectile shown in Fig. 4. Survival has been extrapolated over a time period of 100 s, based on a 1 cm diameter sphere whilst a) radiatively cooling into space and, b) conductively cooling, buried in regolith.

4. Discussion

Quantifying the small fraction of material transferred from the Earth to the Moon via impact ejection requires high-resolution, three-dimensional modelling, due to the disproportionate scale between the large impactor and estimated block size of high-velocity, solid ejecta. Solid blocks of ejecta from km-scale impacts are estimated to be on the order of metres in diameter (Melosh et al., 1992; Wells et al., 2003; Artemieva and Ivanov, 2004; Beech et al., 2019), which is significantly smaller than the 250 m cell sizes currently used in the 100 cppr simulation. Higher still is the resolution needed to fully resolve the fast ejecta ($v_{ej} > 11.2$ km s^{-1}) which experiences the lowest shock-pressures (e.g. Fig. 8 of Artemieva and Ivanov, 2008). The work presented here demonstrates that biomarker survival is expected in many plausible scenarios during the impact of terrestrial material into the Moon. However, from the limited 3D modelling investigating the ejection of material from Earth (Section 3.1), it seems that the launch process may pose a more significant hazard to the biomarkers within terrestrial meteorites than the impact into the lunar surface. Our current models are only able to resolve launched ejecta that has been shocked to pressures greater than 30 GPa; although this ejecta is likely to remain solid, it experiences pressures higher than those compatible with biomarker survival, as demonstrated by the results described in Section 3.2. We expect that there will be solid ejecta which experiences lower shock pressures during launch, based on the lack of convergence in the data (Fig. 1) at the highest resolution attempted so far (100 cppr), but this is unresolved in the simulations presented here. There is also the possibility that a different set of simulation set-up parameters (impact angle, impactor velocity, target material, etc.) would produce more high-speed, low-shock ejecta than the current set-up. Therefore, while the 3D simulations presented here suggest that a small but significant mass of low-shock material is ejected fast enough to transfer from Earth to the Moon in large impacts, further modelling is required to fully quantify the efficiency of impact transfer of material from Earth to the Moon and the survival rates of any biomarkers within that ejected material.

The results presented in this work highlight the need for consideration of both pressure and temperature in the determination of biomarker survival within projectiles that impact the lunar surface, and consideration of temperature is of particular importance when modelling materials with significant strength. Clearly, an important

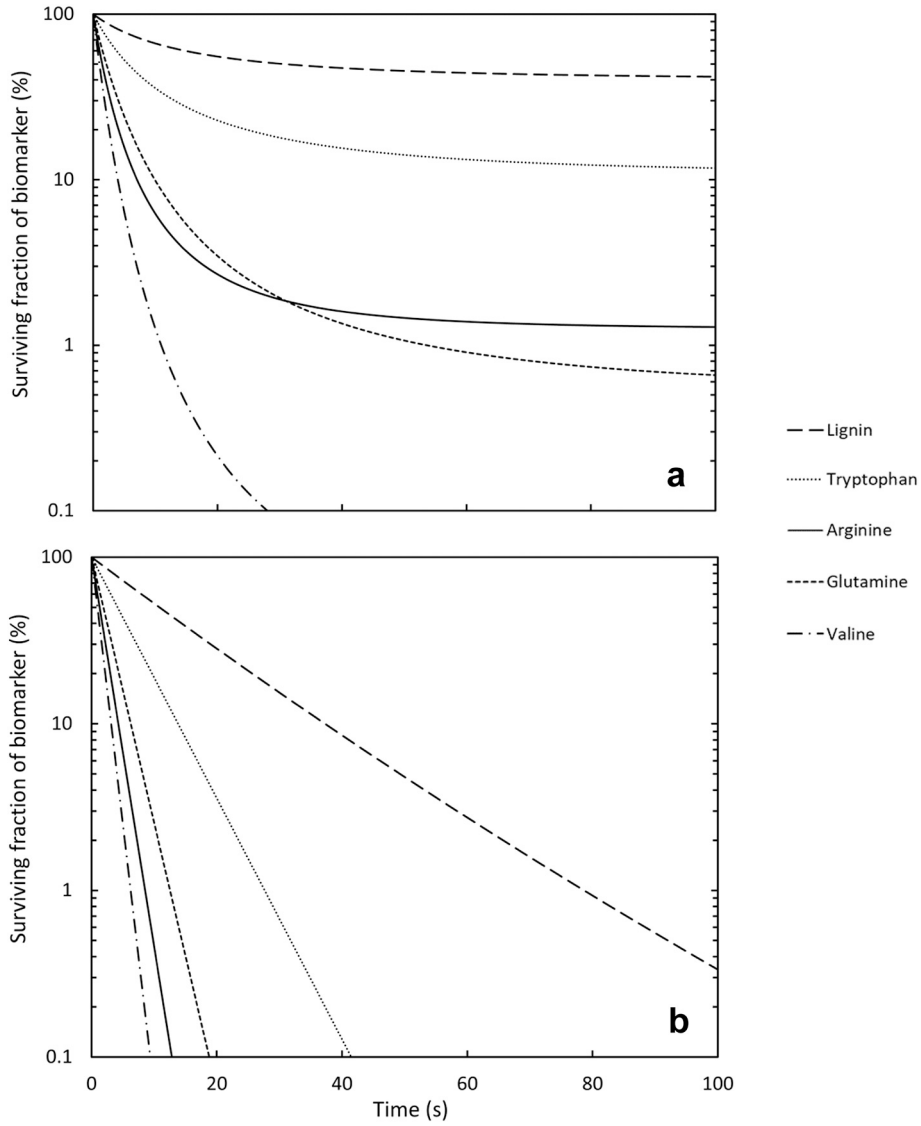

Fig. 7. Survival of selected biomarkers for a tracer that reaches a post-shock temperature of 800 K in part of the sandstone projectile shown in Fig. 5. Survival has been extrapolated over a time period of 100 s, based on a 1 cm diameter sphere whilst a) radiatively cooling into space and, b) conductively cooling, buried in regolith.

consideration for biomarker survival relates to the location of the biomarkers themselves within the projectile. Survival of organic material is not only dependant on the expected pressure and temperatures for a given volume of a projectile (extracted from tracers placed at set intervals within a simulation) but also where the organic material is concentrated within the projectile. The most obvious area for an enhanced probability of survival is as far from the point of contact with the target surface as possible, where pressures and temperatures are at a minimum (Pierazzo and Chyba, 1999; Pierazzo and Melosh, 2000; Potter and Collins, 2013).

There are clear limitations and assumptions when using model tracer information to inform survivability, as the simulations cannot consider the potentially heterogeneous nature of a terrestrial meteorite. For example, if organic material was situated within a pore space at the time of impact then pore collapse will introduce an additional heating component to the usual shock/shear heating process and pressure will be rapidly applied (Wünnemann et al., 2008; Jutzi et al., 2008; Güldemeister et al., 2013) directly to the area where the organic material is located. However, if organic material was surrounded by a dense material within the matrix, or contained within a diaplectic glass as an endogenic melt fragment, the chances of survival upon impact with the lunar surface may be increased (Bland et al., 2014; Davison et al., 2016). More specific consequences for biomarker survivability based upon the heterogeneous nature of polymict geological samples could be explored in future research using mesoscale modelling.

Additionally, it is important to consider the setting where a terrestrial meteorite may land on the lunar surface. Not only will the projectile state and material constrain the pressures and temperatures experienced post-impact, but the target material itself will heavily influence biomarker survivability (Jutzi et al., 2008; Daly and Schultz, 2013; Bruck Syal and Schultz, 2015; Avdellidou et al., 2016) as shown in the various target porosities modelled in this work. Here we have modelled a porous basalt target (broadly representative of the lunar regolith), but what if the terrestrial material impacted a permanently shadowed region (PSR) at the lunar poles? In that case, the role of trapped volatiles would have to be considered in the prospective target (e.g., Watson et al., 1961; Arnold, 1979; Haruyama et al., 2008; Spudis et al., 2008; Zuber et al., 2012). For example, the very low (~40 K; Paige et al., 2009) temperatures experienced by the PSRs would increase the long-term cooling rate of impactor material due to more effective conductive heat-loss. Moreover, the presence of ice in the target layer may enhance projectile survivability: an interstitial regolith-ice mixed target may lead to

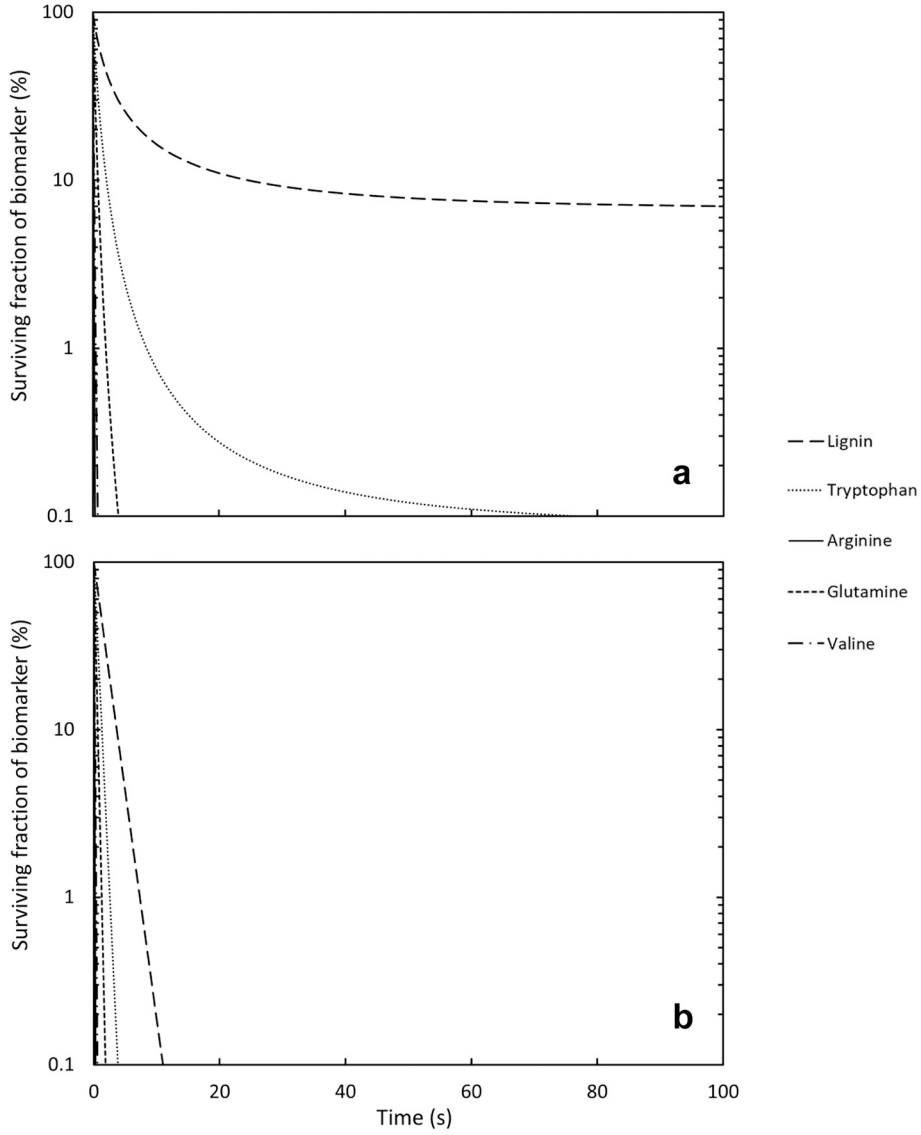

Fig. 8. Survival of selected biomarkers for a tracer that reaches a post-shock temperature of 2000 K in the main body of the sandstone projectile shown in Fig. 5. Survival has been extrapolated over a time period of 100 s, based on a 1 cm diameter sphere whilst a) radiatively cooling into space and, b) conductively cooling, buried in regolith.

projectile material experiencing a dissipation of energy over a greater distance into the target (Avdellidou et al., 2016), which would be beneficial to biomarker survival. Further simulations including interstitially mixed and layered regolith-ice ice targets would be needed to address this question.

Even when modelling results indicate that biomarkers within terrestrial material would survive impacts into the lunar surface, detecting and identifying the surviving material is a challenging prospect (see discussion by Crawford et al., 2008). Survival time of metre-sized boulders on the lunar surface can vary between 10s to 100 s of millions of years (Basilevsky et al., 2013), eventually succumbing to destruction primarily by subsequent impacts and diurnal thermal cycling as a secondary process (Basilevsky et al., 2015). Therefore, if left exposed on the lunar surface, the most abundant and scientifically relevant terrestrial examples from the LHB ~3.9 Ga ago would have been destroyed long ago. On the other hand, rapid burial of terrestrial meteorites by crater and basin ejecta, and/or by mare basalt flows, could have potentially provided protection for this material (e.g., Crawford and Joy, 2014; Joy et al., 2016). Indeed, recent experimental work (Matthewman et al., 2015, 2016) suggests that burial in lunar regolith will help preserve a range of potential organic molecules. Later exhumation by impact gardening of the lunar regolith would then allow for buried terrestrial material to be present on or near the surface at present day, where it might be detected spectroscopically (see discussion by Crawford et al., 2008 and Joy et al., 2016). Preservation of terrestrial material would presumably be maximised if it remained buried, but in that case the only hope of detecting it would be as chance discoveries in drill core samples of palaeoregolith deposits collected for other purposes (Crawford and Joy, 2014).

Finally we note that if, as argued by Needham and Kring (2017), the Moon had a thin (~10 mbar) atmosphere at the time of peak mare volcanism (~3.8 Ga, just after the LHB on the Moon but at a time when giant impacts may have been continuing on the Earth) the survival of terrestrial meteorites on the Moon would be potentially enhanced owing to atmospheric deceleration prior to impact; this would be an interesting topic for future investigation.

5. Conclusions

Previous studies (Armstrong et al., 2002; Gutiérrez, 2002; Crawford

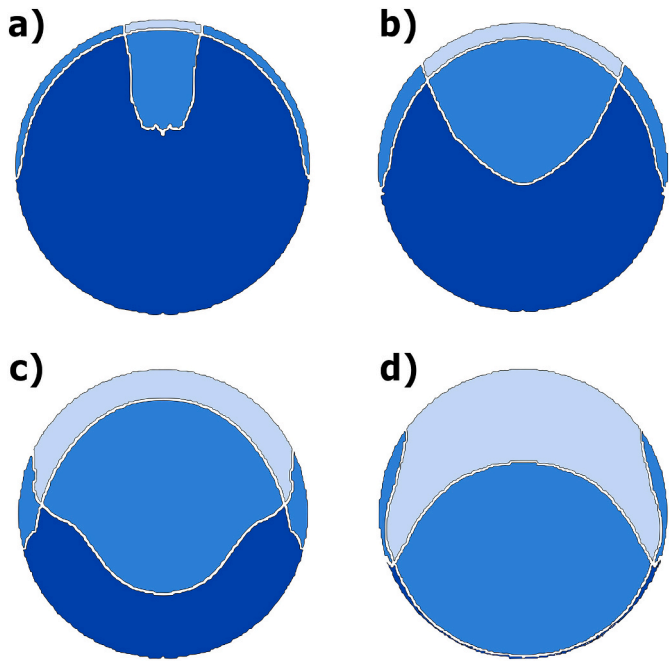

Fig. 9. Contour plots showing regions of the projectile where lycophyte megaspores are likely to survive after impact. Projectiles were all solid, impacting at 2.5 km s^{-1} into targets with varying porosity: a) 0% (solid), b) 30%, c) 50%, d) 70%. Lightest colour = both pressure and temperature favourable for survival, intermediate = pressure or temperature not favourable for survival, darkest = both pressure and temperature unfavourable for survival.

et al., 2008; Armstrong, 2010; Beech et al., 2019) have indicated that fragments of the Earth's crust may have been ejected by large impacts and transferred to the Moon as terrestrial meteorites. The survivability of biomarkers from the early Earth in such material would be of great scientific interest. In this paper we report two- and three-dimensional hydrocode modelling to show that a fraction of terrestrial impact ejecta (amounting to <0.13% of the mass of impactors striking Earth) may escape Earth having been subjected to sufficiently low pressures to remain solid and that this material therefore has the potential to reach the Moon. Assuming that any biomarkers entrained within this material can survive ejection from the Earth (which will need to be confirmed in future work), we have shown that a range of plausible biomarkers have the potential to survive impact on the lunar surface.

At the maximum impact velocity for terrestrial meteorites impacting the Moon (5 km s^{-1}) or less, peak temperatures across the projectile are significantly higher when projectile strength is accounted for compared with the strengthless scenario in which heating is caused exclusively by shock compression. This supports findings in previous studies in target materials (Quintana et al., 2015; Kurosawa and Genda, 2018) and shows shear heating can have an important effect in projectile material. Comparison with previous work (Crawford et al., 2008), which neglected shear heating, indicates reduced survivability in models with 5 km s^{-1} projectile velocity due to higher peak temperatures within the projectile. Temperatures near the contact zone reach those required for melting and vaporisation of the projectile itself, especially when a porous projectile impacts a solid target.

Lower impact velocity (2.5 km s^{-1}), lower projectile porosity, and/or higher target porosity, increases the likelihood of survival for the projectile and any organic molecules within them. The most favourable conditions for survivability involve a solid projectile, impacting at low velocity (2.5 km s^{-1}) into a highly porous (50–70%) regolith. In this case, even lycophyte megaspores are expected to survive with little to no alteration based on their survival pressures and temperatures in metamorphosed samples. Our results show that this would be the case for both sandstone and limestone projectiles, with limestone having a somewhat greater potential for biomarker survival than sandstone.

Post-impact cooling timescales depends heavily on the final location and size of the surviving fragments. Small (cm-scale) fragments which are ejected and land on the lunar surface will cool quickly (seconds) by radiation, leading to the most favourable conditions for biomarker material. Lignin and tryptophan have been shown to survive well in these conditions across the range of impact scenarios simulated in this work. Buried projectile fragments will cool over much longer timescales (days) by conduction leading to conditions in which no biomarkers would survive, even in the most favourable impact scenarios simulated in this work. Larger (tens of cm to metre-scale) fragments will cool slower, regardless of the cooling process, leading to less favourable conditions for biomarker survival. After their initial cooling, the survival of biomarkers over a geological timescale (millions to billions of years) will be dependent on the subsequent burial of biomarker rich projectile fragments by ejecta from later impacts or lava flows. These will act as an insulating layer to protect the surviving biomarkers from fluctuating surface temperatures and cosmic radiation.

Given that most terrestrial meteorites currently residing on the Moon will have been launched from the Earth during the first billion years of Solar System history, when impact fluxes were highest, they have the potential to provide astrobiologically important information on a period of Earth's early geological and biological evolution that Earth itself no longer retains. These conclusions imply that a search for terrestrial meteorites on the Moon should join the already long list of scientific reasons for resuming the exploration of the lunar surface (e.g., NRC, 2007; Crawford and Joy, 2014; LEAG, 2016; Tartèse et al., 2019).

Declaration of Competing Interest

None.

Acknowledgements

We gratefully thank Boris Ivanov, Jay Melosh, Kai Wünnemann, Dirk Elbeshausen for their work in the development of iSALE. Samuel Halim would like to acknowledge STFC for funding through the award of a post-graduate studentship. KHJ acknowledges STFC (ST/M001253/1) and the Royal Society (RS/UF140190). KHJ and IAC acknowledge Leverhulme Trust (RPG-2019-222). GSC and TMD were funded by STFC Grant ST/S000615/1. This work was performed in part using the DiRAC Data Intensive service at Leicester, operated by the University of Leicester IT Services, which forms part of the STFC DiRAC HPC Facility (www.dirac.ac.uk). The equipment was funded by BEIS capital funding via STFC capital grants ST/K000373/1 and ST/R002363/1 and STFC DiRAC Operations grant ST/R001014/1. DiRAC is part of the National e-Infrastructure. We thank Editor-in-Chief, Dr. Rosaly Lopes for editorial handling, as well as Dr. Natalia Artemieva and an anonymous reviewer for improving this manuscript with their helpful suggestions.

Appendix A. Supplementary data

Supplementary data to this article can be found online at https://doi.org/10.1016/j.icarus.2020.114026.

References

Amsden, A., Ruppel, H., Hirt, C., 1980. SALE: a simplified ALE computer program for fluid flow at all speeds. LANL Rep.. LA-8095.
Armstrong, J., 2010. Distribution of impact locations and velocities of Earth meteorites on the Moon. Earth Moon Planet. 107 (1), 43–54.
Armstrong, J., Wells, L., Gonzalez, G., 2002. Rummaging through Earth's attic for remains of ancient life. Icarus 160 (1), 183–196. https://doi.org/10.1006/icar.2002.6957.
Arnold, J.R., 1979. Ice in the lunar polar regions. J. Geophys. Res. 84, 5659–5668.
Artemieva, N.A., Ivanov, B.A., 2004. Launch of martian meteorites in oblique impacts. Icarus 171, 84–101. https://doi.org/10.1016/j.icarus.2004.05.003.

Artemieva, N.A., Morgan, J., 2009. Modeling the formation of the K–Pg boundary layer. Icarus 201 (2), 768–780. https://doi.org/10.1016/j.icarus.2009.01.021.

Avdellidou, C., Price, M., Delbo, M., Cole, M., 2016. Survival of the impactor during hypervelocity collisions – II. An analogue for high-porosity targets. Mon. Not. R. Astron. Soc. 464 (1), 734–738. https://doi.org/10.1093/mnras/stw2381.

Basilevsky, A., Head, J., Horz, F., 2013. Survival times of meter-sized boulders on the surface of the Moon. Planet.Space Sci.e 89, 118–126.

Basilevsky, A., Head, J., Horz, F., Ramsley, K., 2015. Survival times of meter-sized rock boulders on the surface of airless bodies. Planet. Space Sci. 117, 312–328.

Beech, M., Comte, M., Coulson, I., 2019. The production of terrestrial meteorites – Moon accretion and Lithopanspermia. Am. J. Astron. Astrophys. 7 (1), 1–9.

Bellucci, J., et al., 2019. Terrestrial-like zircon in a clast from an Apollo 14 breccia. Earth Planet. Sci. Lett. 510, 173–185.

Bernard, S., Benzerara, K., Beyssac, O., Menguy, N., Guyot, F., Brownjr, G., Goffe, B., 2007. Exceptional preservation of fossil plant spores in high-pressure metamorphic rocks. Earth Planet. Sci. Lett. 262 (1–2), 257–272. https://doi.org/10.1016/j.epsl.2007.07.041.

Bertrand, M., et al., 2009. The fate of amino acids during simulated meteoritic impact. Astrobiology 9 (10), 943–951. https://doi.org/10.1089/ast.2008.0327.

Bland, P.A., Artemieva, N.A., Collins, G.S., Bottke, W.F., Bussey, D.B.J., Joy, K.H., 2008. Asteroids on the moon: projectile survival during low velocity impact. Lunar Planet. Sci. XXXIX abstract #2045.

Bland, P., Collins, G., Davison, T., et al., 2014. Pressure–temperature evolution of primordial solar system solids during impact-induced compaction. Nat. Commun. 5, 5451. https://doi.org/10.1038/ncomms6451.

Bottke, W.F., et al., 2012. An Archaean heavy bombardment from a destabilized extension of the asteroid belt. Nature 485, 78–81.

Brebu, M., Vasile, C., 2010. Thermal degradation of lignin – a review. Cellul. Chem. Technol. 44, 353–363.

Bruck Syal, M., Schultz, P.H., 2015. Impact delivery of water at the Moon and Mercury. Lunar Planet. Sci. XXXXVI. Abstract #1680.

Burchell, M., Bowden, S., Cole, M., Price, M., Parnell, J., 2014a. Survival of organic materials in hypervelocity impacts of ice on sand, ice, and water in the laboratory. Astrobiology 14 (6), 473–485.

Burchell, M., Harriss, K., Price, M., Yolland, L., 2017. Survival of fossilised diatoms and forams in hypervelocity impacts with peak shock pressures in the 1–19 GPa range. Icarus 290, 81–88. https://doi.org/10.1016/J.ICARUS.2017.02.028.

Burchell, M., McDermott, K., Price, M., Yolland, L., 2014b. Survival of fossils under extreme shocks induced by hypervelocity impacts. Philos. Trans. R. Soc. A Math. Phys. Eng. Sci. 372, 20130190.

Carrier III, W.D., Olhoeft, G.R., Mendell, W., 1991. Physical properties of the lunar surface. In: Heiken, G.H., Vaniman, D.T., French, B.M. (Eds.), Lunar Sourcebook–A User's Guide to the Moon. Cambridge University Press, Cambridge, pp. 475–594. Available online at: https://www.lpi.usra.edu/publications/books/lunar_sourcebook/pdf/Chapter09.pdf.

Cohen, B.A., Swindle, T.D., Kring, D.A., 2000. Support for the lunar cataclysm hypothesis from lunar meteorite impact melt ages. Science 290 (5497), 1754–1756.

Collins, G.S., Melosh, H.J., Ivanov, B.A., 2004. Modeling damage and deformation in impact simulations. Meteorit. Planet. Sci. 39 (2), 217–231.

Collins, G.S., Patel, N., Davison, T.M., Rae, A.S.P., Morgan, J.V., Gulick, S.P.S., 2020. A steeply-inclined trajectory for the Chicxulub impact. Nat. Commun. 11, 1480. https://doi.org/10.1038/s41467-020-15269-x.

Crawford, I.A., Joy, K.H., 2014. Lunar exploration: opening a window into the history and evolution of the inner solar system. Phil. Trans. R. Soc. A 372, 20130315.

Crawford, I.A., Baldwin, E., Taylor, E., Bailey, J., Tsembelis, K., 2008. On the survivability and detectability of terrestrial meteorites on the moon. Astrobiology 8, 242–252.

Daly, R.T., Schultz, P.H., 2013. Experimental studies into the survival and state of the projectile. Lunar Planet. Sci. XXXXIV. Abstract #2240.

Daly, R.T., Schultz, P.H., 2015. Predictions for impactor contamination on Ceres based on hypervelocity impact experiments. Geophys. Res. Lett. 42 (19), 7890–7898.

Davison, T.M., Collins, G.S., Elbeshausen, D., Wünnemann, K., Kearsley, A., 2011. Numerical modeling of oblique hypervelocity impacts on strong ductile targets. Meteorit. Planet. Sci. 46 (10), 1510–1524.

Davison, T.M., Collins, G.S., Bland, P.A., 2016. Mesoscale modeling of impact compaction of primitive solar system solids. Astrophys. J. 821 (1), 68. https://doi.org/10.3847/0004-637x/821/1/68.

Day, J.M.D., Floss, C., Taylor, L.A., Anand, M., Patchen, A.D., 2006. Geochim. Cosmochim. Acta 70, 5957–5989.

Elbeshausen, D., Wünnemann, K., 2011. iSALE-3D: a three-dimensional, multi- material, multi-rheology hydrocode and its applications to large scale geodynamic processes. In: Proceedings of 11th Hypervelocity Impact Symposium 287±301.

Elbeshausen, D., Wünnemann, K., Collins, G.S., 2009. Scaling of oblique impacts in frictional targets: implications for crater size and formation mechanisms. Icarus 204, 716–731. https://doi.org/10.1016/j.icarus.2009.07.018.

Fagents, S., Elise Rumpf, M., Crawford, I.A., Joy, K.J., 2010. Preservation potential of implanted solar wind volatiles in lunar paleoregolith deposits buried by lava flows. Icarus 207 (2), 595–604. https://doi.org/10.1016/j.icarus.2009.11.033.

Goldin, T., Wünnemann, K., Melosh, H., Collins, G., 2006. Hydrocode modeling of the Sierra Madera impact structure. Meteorit. Planet. Sci. 41 (12), 1947–1958. https://doi.org/10.1111/j.1945-5100.2006.tb00462.x.

Goldstein, J.I., Henderson, E.P., Yakowitz, H., 1970. Investigation of Lunar Metal Particles. *Geochimica et Cosmochimica Acta Supplement*, Volume 1. In: Levinson, A.A. (Ed.), Proceedings of the Apollo 11 Lunar Science Conference, Houston, TX. Volume 1: Mineralogy and Petrology. Pergammon Press, New York, pp. 499–512, 1970.

Gomes, R., Levison, H., Tsiganis, K., Morbidelli, A., 2005. Origin of the cataclysmic Late Heavy Bombardment period of the terrestrial planets. Nature 435 (7041), 466–469.

Güldemeister, N., Wünnemann, K., Durr, N., Hiermaier, S., 2013. Propagation of impact-induced shock waves in porous sandstone using mesoscale modeling. Meteorit. Planet. Sci. 48, 115–133. https://doi.org/10.1111/j.1945-5100.2012.01430.x.

Gutiérrez, J.L., 2002. Terrene meteorites in the Moon: their relevance for the study of the origin of life in the Earth. ESA SP-518, 187–191.

Hartmann, W., 1975. Lunar "cataclysm": a misconception? Icarus 24 (2), 181–187. https://doi.org/10.1016/0019-1035(75)90095-0.

Hartmann, W., 2003. Megaregolith evolution and cratering cataclysm models-Lunar cataclysm as a misconception (28 years later). Meteorit. Planet. Sci. 38 (4), 579–593.

Hartmann, W., 2019. History of the terminal cataclysm paradigm: epistemology of a planetary bombardment that never (?) happened. Geosciences 9 (7), 285. https://doi.org/10.3390/geosciences9070285.

Haruyama, J., Ohtake, M., Matsunaga, T., Morota, T., Honda, C., Yokota, Y., 2008. Lack of exposed ice inside lunar south pole Shackleton crater. Science 322 (5903), 938–939. https://doi.org/10.1126/science.1164020.

Jolliff, B.L., Korotev, R.L., Haskin, L.A., 1993. An iridium-rich iron micrometeorite with silicate inclusions from the Moon. Lunar Planet. Sci. XXIV. Abstract #1366.

Joy, K.H., Zolensky, M.E., Nagashima, K., Huss, G.R., McKay, D.S., Ross, D.S., Kring, D. A., 2012. Direct Detection of Projectile Relics from the End of the Lunar Basin–Forming Epoch. Science 336, 1426–1429. https://doi.org/10.1126/science.1219633.

Joy, K.H., Crawford, I.A., Curran, N., Zolensky, M., Fagan, A., Kring, D.A., 2016. The Moon: an archive of small body migration in the solar system. Earth Moon Planet. 118 (2–3), 133–158.

Joy, K.H., Tartèse, R., Messenger, S., Zolensky, M.E., Marrocchi, Y., Frank, D.R., Kring, D. A., 2020. The isotopic composition of volatiles in the unique bench crater carbonaceous chondrite impactor found in the Apollo 12 regolith. Earth Planet. Sci. Lett. 540, 116265. https://doi.org/10.1016/j.epsl.2020.116265.

Jutzi, M., Benz, W., Michel, P., 2008. Numerical simulations of impacts involving porous bodies. Icarus 198 (1), 242–255. https://doi.org/10.1016/j.icarus.2008.06.013.

Kurosawa, K., Genda, H., 2018. Effects of friction and plastic deformation in shock-comminuted damaged rocks on impact heating. Geophys. Res. Lett. 45 (2), 620–626.

Laborda-López, C., Aguirre, J., Donovan, S., 2015. Surviving metamorphism: taphonomy of fossil assemblages in marble and calc-silicate schist. Palaios 30 (9), 668–679. https://doi.org/10.2110/palo.2015.013.

Le Feuvre, M., Wieczorek, M.A., 2011. Nonuniform cratering of the Moon and a revised crater chronology of the inner solar system. Icarus 214, 1–20. https://doi.org/10.1016/j.icarus.2011.03.010.

Lienhard, J.H., Lienhard, J.H., 2001. A Heat Transfer Textbook, Third edition. Phlogiston Press, Cambridge, Massachusetts, USA. Available at: http://www.mie.uth.gr/labs/ltte/grk/pubs/ahtt.pdf.

Liu, Y., Zhang, A., Taylor, L.A., 2009. Fragments of Asteroids in Lunar Rocks. In: 72nd Annual Meteoritical Society Meeting. Abstract #5434.

Lunar Exploration Analysis Group (LEAG), 2016. The Lunar Exploration Roadmap: Exploring the Moon in the 21st Century: Themes, Goals, Objectives, Investigations, and Priorities..

Marchi, S., Bottke, W., Kring, D.A., Morbidelli, A., 2012. The onset of the lunar cataclysm as recorded in its ancient crater populations. Earth Planet. Sci. Lett. 325–326, 27–38. https://doi.org/10.1016/j.epsl.2012.01.021.

Marchi, S., Bottke, W.F., Elkins-Tanton, L.T., Bierhaus, M., Wuennemann, K., Morbidelli, A., Kring, D.A., 2014. Widespread mixing and burial of Earth's hadean crust by asteroid impacts. Nature 511, 578–582.

Matthewman, R., Court, R.W., Crawford, I.A., Jones, A.P., Joy, K.H., 2015. The Moon as a recorder of organic evolution in the early solar system: a lunar regolith analog study. Astrobiology 15, 154–168.

Matthewman, R., Crawford, I.A., Jones, A.P., Joy, K.H., Sephton, M.A., 2016. Organic matter responses to radiation under lunar conditions. Astrobiology 16, 900–912.

McKay, D.S., Carter, J.L., Greenwood, W.R., 1970. Science 171, 479–480.

Melosh, H.J., 1984. Impact ejection, spallation, and the origin of meteorites. Icarus 59 (2), 234–260. https://doi.org/10.1016/0019-1035(84)90026-5.

Melosh, H.J., 1985. Ejection of rock fragments from planetary bodies. Geology 13 (2), 144–148. https://doi.org/10.1130/0091-7613(1985)13<144:EORFFP>2.0.CO;2.

Melosh, H.J., 1989. Impact Cratering: A Geologic Process. Oxford Univ, Clarendon, Oxford.

Melosh, H.J., 2007. A hydrocode equation of state for SiO_2. Meteoritics & Planetary Science 42 (12), 2079–2098. https://doi.org/10.1111/j.1945-5100.2007.tb01009.x.

Melosh, H.J., Ivanov, B.A., 2018. Slow impacts on strong targets bring on the heat. Geophys. Res. Lett. 45 (6), 2597–2599. https://doi.org/10.1002/2018gl077726.

Melosh, H.J., Ryan, E., Asphaug, E., 1992. Dynamic fragmentation in impacts: Hydrocode simulation of laboratory impacts. JGR 97, 14735. https://doi.org/10.1029/92je01632.

Meyer, C., et al., 2011. Shock experiments in support of the Lithopanspermia theory: the influence of host rock composition, temperature, and shock pressure on the survival rate of endolithic and epilithic microorganisms. Meteorit. Planet. Sci. 46 (5), 701–718. https://doi.org/10.1111/j.1945-5100.2011.01184.x.

Mimura, K., Toyama, S., 2005. Behavior of polycyclic aromatic hydrocarbons at impact shock: its implication for survival of organic materials delivered to the early earth. Geochim. Cosmochim. Acta 69 (1), 201–209.

Morbidelli, A., Marchi, S., Bottke, W.F., Kring, D.A., 2012. A sawtooth-like timeline for the first billion years of lunar bombardment. Earth Planet. Sci. Lett. 355, 144–151.

National Research Council (NRC), 2007. The Scientific Context for Exploration of the Moon, Final Report, National Academy Press, Washington, D. C.

Nave, R., 2017. Radiative cooling time. In: Hyperphysics. Georgia State University. Retrieved 24 January 2020, from. http://hyperphysics.phy-astr.gsu.edu/hbase/thermo/cootime.html.
Needham, D.H., Kring, D.A., 2017. Lunar volcanism produced a transient atmosphere around the ancient Moon. Earth Planet. Sci. Lett. 478, 175–178.
Nelson, J.B., 1967. Thermogravimetric Analysis of Ablating Polymers to Determine Kinetic Parameters Describing Mass Loss due to Thermal Degradation. In: NASA Technical Report. NASA Langley Research Center, Hampton, VA, pp. 1–19. ID: 19670013969.
Norman, M.D., 2009. The lunar cataclysm: reality or "mythconception". Elements 5, 23–28.
Ong, L., Asphaug, E., Korycansky, D., Coker, R., 2010. Volatile retention from cometary impacts on the moon. Icarus 207 (2), 578–589. https://doi.org/10.1016/j.icarus.2009.12.012.
Paige, D., et al., 2009. The lunar reconnaissance orbiter diviner lunar radiometer experiment. Space Sci. Rev. 150 (1–4), 125–160.
Parnell, J., et al., 2010. The preservation of fossil biomarkers during meteorite impact events: experimental evidence from biomarker-rich projectiles and target rocks. Meteorit. Planet. Sci. 45 (8), 1340–1358.
Peters, K., Walters, C., Moldowan, J., 2004. The Biomarker Guide. Cambridge University Press, Cambridge. https://doi.org/10.1017/CBO9781107326040.
Pierazzo, E., Chyba, C., 1999. Amino acid survival in large cometary impacts. Meteorit. Planet. Sci. 34 (6), 909–918. https://doi.org/10.1111/j.1945-5100.1999.tb01409.x.
Pierazzo, E., Chyba, C., 2002. Cometary delivery of biogenic elements to Europa. Icarus 157 (1), 120–127. https://doi.org/10.1111/j.1945-5100.1999.tb01409.x.
Pierazzo, E., Melosh, H., 2000. Hydrocode modeling of oblique impacts: the fate of the projectile. Meteorit. Planet. Sci. 35 (1), 117–130.
Pierazzo, E., Vickery, A.M., Melosh, H.J., 1997. A reevaluation of impact melt production. Icarus 127 (2), 408–423. https://doi.org/10.1006/icar.1997.5713.
Pierazzo, E., Kring, D., Melosh, H., 1998. Hydrocode simulation of the Chicxulub impact event and the production of climatically active gases. J. Geophys. Res. Planet. 103 (E12), 28607–28625. https://doi.org/10.1029/98je02496.
Pierazzo, E., Artemieva, N.A., Ivanov, B.A., 2005. Starting conditions for hydrothermal systems underneath Martian Craters: hydrocode modeling. In: Kenkmann, T., Hörz, F., Deutsch, A. (Eds.), Large Meteorite Impacts III. Geological Society of America, Boulder, CO, pp. 443–457.
Potter, R., Collins, G., 2013. Numerical modeling of asteroid survivability and possible scenarios for the Morokweng crater-forming impact. Meteorit. Planet. Sci. 48 (5), 744–757.
Quaide, W., Bunch, T., 1970. Geochimica et Cosmochimica Acta Suppl., 1, pp. 711–729. Proceedings of the Apollo 11 Lunar Science Conference.
Quintana, S., Crawford, D., Schultz, P., 2015. Analysis of impact melt and vapor production in CTH for planetary applications. Procedia Eng. 103, 499–506. https://doi.org/10.1016/j.proeng.2015.04.065.
Rodante, F., 1992. Thermodynamics and kinetics of decomposition processes for standard α-amino acids and some of their dipeptides in the solid state. Thermochim. Acta 200, 47–61. https://doi.org/10.1016/0040-6031(92)85105-5.
Schultz, P., Hermalyn, B., Colaprete, A., Ennico, K., Shirley, M., Marshall, W., 2010. The LCROSS cratering experiment. Science 330 (6003), 468–472.
Shaw, C., 2019. Metamorphic mineral assemblages in fossils in the contact metamorphic rocks of the Portrush Sill, Northern Ireland. Lithos 338-339, 99–110. https://doi.org/10.1016/j.lithos.2019.04.016.
Shoemaker, E.M., 1962. Interpretation of lunar craters. In: Kopal, A. (Ed.), Physics and Astronomy of the Moon. Academic Press, New York, pp. 283–351.
Spudis, P., Bussey, B., Plescia, J., Josset, J., Beauvivre, S., 2008. Geology of Shackleton crater and the south pole of the Moon. Geophys. Res. Lett. 35 (14) https://doi.org/10.1029/2008GL034468.
Stöffler, D., Ryder, G., Ivanov, B.A., Artemieva, N.A., Cintala, M.A., Grieve, R.A.F., 2006. Cratering history and lunar chronology. Rev. Mineral. Geochem. 60, 519–596.
Svetsov, V., Shuvalov, V., 2015. Water delivery to the Moon by asteroidal and cometary impacts. Planetary & Space Science 117, 444–452.
Tartèse, R., et al., 2019. Constraining the evolutionary history of the moon and the inner solar system: a case for new returned lunar samples. Space Sci. Rev. 215, 54. https://doi.org/10.1007/s11214-019-0622-x.
Tera, F., Papanastassiou, D., Wasserburg, G., 1974. Isotopic evidence for a terminal lunar cataclysm. Earth Planet. Sci. Lett. 22 (1), 1–21.
Thompson, S.L., Lauson, H.S., 1972. Improvements in the Chart-D Radiation Hydrodynamic Code III: Revised Analytical Equation of State: Sandia Laboratories Report SC-RR-71 0714, 119.
Turner, G., 1979. A Monte Carlo Fragmentation Model for the Production of Meteorites – Implications for Gas Retention Ages. Lunar and Planetary Science Conference, 10th, Houston, March 19–23, Proceedings, vol 2. Pergamon Press, New York, pp. 1917–1941. A80-23617 08-91.
Turner, G., Cadogan, P.H., Yonge, C.J., 1973. Argon selenochronology. In: Proceedings, 4th Lunar Science Conference, Houston, pp. 1889–1914.
Warren, P.H., Rubin, A.E., 2020. Trace element and textural evidence favoring lunar, not terrestrial, origin of the mini-granite in Apollo sample 14321. Icarus 347, 113771. https://doi.org/10.1016/j.icarus.2020.113771.
Watson, K., Murray, B.C., Brown, H., 1961. The behavior of volatiles on the lunar surface. J. Geophys. Res. 66, 3033–3045.
Wells, L., Armstrong, J., Gonzalez, G., 2003. Reseeding of early earth by impacts of returning ejecta during the late heavy bombardment. Icarus 162 (1), 38–46. https://doi.org/10.1016/S0019-1035(02)00077-5.
Wickham-Eade, J., Burchell, M., Price, M., Harriss, K., 2018. Hypervelocity impact fragmentation of basalt and shale projectiles. Icarus 311, 52–68. https://doi.org/10.1016/j.icarus.2018.03.017.
Wood, J.A., Marvin, U.B., Reed, J.B., Taylor, G.J., Bower, J.F., Powell, B.N., Dickey, J.S., 1971. Mineralogy and petrology of the Apollo 12 lunar sample. Smithsonian Astrophys. Obs. Spec. Rep. 333, 177.
Wünnemann, K., Collins, G.S., Melosh, H., 2006. A strain-based porosity model for use in hydrocode simulations of impacts and implications for transient crater growth in porous targets. Icarus 180 (2), 514–527. https://doi.org/10.1016/j.icarus.2005.10.013.
Wünnemann, K., Collins, G.S., Osinski, G., 2008. Numerical modelling of impact melt production in porous rocks. Earth Planet. Sci. Lett. 269 (3–4), 530–539.
Yue, Z., Johnson, B., Minton, D., Melosh, H., Di, K., Hu, W., Liu, Y., 2013. Projectile remnants in central peaks of lunar impact craters. Nat. Geosci. 6 (6), 435–437.
Zellner, N.E.B., 2017. Cataclysm no more: new views on the timing and delivery of lunar impactors. Orig. Life Evol. Biosph. 47, 261–280.
Zolensky, M.E., Weisberg, M.K., Buchanan, P.C., Mittlefehldt, D.W., 1996. Mineralogy of carbonaceous chondrite clasts in HED achondrites and the Moon. Meteorit. Planet. Sci. 31, 518–537.
Zuber, M.T., et al., 2012. Constraints on the volatile distribution within Shackleton crater at the lunar south pole. Nature 486, 378–381. https://doi.org/10.1038/nature11216.